*J. Fluid Mech.* (2005), *vol.* 527, *pp.* 197–216.  
DOI: 10.1017/S0022112004003064 Printed in the United Kingdom

# Experimental study of a surfactant-driven fingering phenomenon in a Hele-Shaw cell

By J. FERNANDEZ†, R. KRECHETNIKOV AND G. M. HOMSY

University of California, Santa Barbara, CA 93106, USA

(Received 15 March 2004 and in revised form 25 September 2004)

We present an experimental study of a new surfactant-driven fingering phenomenon in a Hele-Shaw cell. First, the threshold of instability is examined and compared with the linear theory. Second, the nonlinear evolution of fingering is quantified, and steady and unsteady patterns are distinguished. A wide range of dynamical behaviour is observed from drifting and merging fingers to cusp formation between fingers and subsequent ejection of air bubbles. All experiments are performed with a pure surfactant – sodium dodecyl sulphate – thus allowing us to obtain a well-defined bifurcation map for the specific kinetic and material properties of this surface-active substance. The measurements are conducted in a Hele-Shaw cell with smooth and roughened walls. A basic physical model is proposed to obtain further insight into the influence of the surfactant properties on the dip-coating process and, as a result, on the critical phenomena. The study allows us to resolve the discrepancies between previous experimental results and linear theory.

## 1. Introduction

The discovery by Chan & Liang (1997) of a new type of instability in a well-studied physical set-up – a Hele-Shaw cell – in the presence of a pre-existing wetting layer of surfactant offers new perspectives for studying fundamental aspects of surfactant-driven hydrodynamic instabilities as well as surfactant material behaviour. We refer the reader to Krechetnikov & Homsy (2004) for a detailed discussion of this phenomenon in the context of Marangoni-driven instabilities and for the history of the problem. While the linear stability properties of this new phenomenon have been studied in the above cited work, some discrepancies between the experimental results by Chan & Liang (1997) and our theoretical predictions were revealed. This makes it necessary to conduct further experiments in order to test the predictions of the theory and perform a more extensive study of the nonlinear regimes of the instability.

First, we remind the reader of the main results by Chan & Liang (1997). Their experiments were performed in a Hele-Shaw cell of 300 μm gap width with three types of surfactants: two commercial soap detergents – Moore Dish Wash (MDW), which is a mixture of three components, and a two-component soap (Salatt detergent) – and pure sodium dodecyl sulphate (SDS). First a wetting layer of surfactant solution was deposited on the inner walls by withdrawing the cell from a bath of surfactant solution. Then, the coated cell was driven into the same surfactant solution at a constant speed

† Present address: Dpto. de Ingenieria Energetica y Mecanica de Fluidos Institution, Universidad de Sevilla Avenida de los Cartuja, 41092 Sevilla, Spain.

and it was observed that the air/liquid interface is unstable under specific conditions: (*a*) the speed of driving should be above a critical velocity (below which the interface remains essentially flat), and (*b*) the surfactant concentration must be above the critical micellar concentration (CMC). It was also found that the instability occurs only for SDS or MDW solutions. In the nonlinear regime, Chan & Liang (1997) observed that the fingering patterns reaches a steady state, with blunted fronts and sharp tails pointing in the direction opposite to the interface motion. One peculiarity of this phenomenon is its apparent contradiction to the linear stability analysis by Saffman & Taylor (1958) of the viscous fingering instability, which predicts that the interface between a fluid displacing a less viscous one is always stable.

Chan (2000) hypothesized that this new instability is due to the accumulation of surfactants at the advancing interface and the diffusion of surfactants in the wetting layer, but did not provide an analysis that would support or refute this hypothesis. Krechetnikov & Homsy (2004) performed a linear stability analysis to explain the experimental observations of Chan & Liang (1997) and to reveal the instability mechanism. In particular, the crucial effect of the pre-existing wetting layer of surfactant was identified: the instability is due to the thickening of the wetting layer induced by Marangoni stresses which originate from the accumulation of surfactants in the cap region of the meniscus as it is driven into the cell. The presence of the wetting layer and of an advancing meniscus is crucially important for producing the instability. A striking discrepancy between the theory and previous experiments by Chan & Liang (1997) is that the former predicts instability only for concentrations below CMC, while the latter claims it only occurs above CMC.

In the present work, we study carefully the variation of the critical speed for the onset of the instability over the full range of two key parameters, the bulk surfactant concentration and the speed of withdrawal of the plates. The details of the experimental setup and properties of the single molecule surfactant used in our experiments are given in § 2. In § 3 we discuss the experiments performed near the threshold of instability and compare them with the conclusions drawn by Chan & Liang (1997), in particular that the instability occurs only for bulk concentrations above CMC. Section 4 is devoted to a comparison with the linear theory by Krechetnikov & Homsy (2004). Finally, in § 5, we describe the fingering dynamics observed in the nonlinear regime.

## 2. Basic description of experiments

### 2.1. *Experimental setup and procedure*

The experiments are conducted in the vertical Hele-Shaw cell sketched in figure 1. Two glass plates of 64 cm long and 15 cm wide are held together by clamps which are regularly spaced in order to maintain a uniform gap. The gap thickness is fixed by two plastic shims (2.5 cm wide and 64 cm long) 310 μm thick placed between the plates at both borders. We suspend the cell vertically on a two-rail translation stage controlled by a stepper motor (Velmex) producing speeds ranging from 0.127 to 3.87 cm $s^{-1}$. A Plexiglas tank containing an aqueous solution of surfactant is placed underneath the cell.

The experimental procedure is as follows. The dry cell is first lowered into the tank and then withdrawn at a constant speed $V_d$, thus depositing a wetting layer on the plates as shown schematically in figure 1. The thickness of this film is determined by the relative speed of the plate and the meniscus and by the surfactant dynamics. We conducted experiments over a range of capillary numbers between $10^{-5}$ and $10^{-3}$,

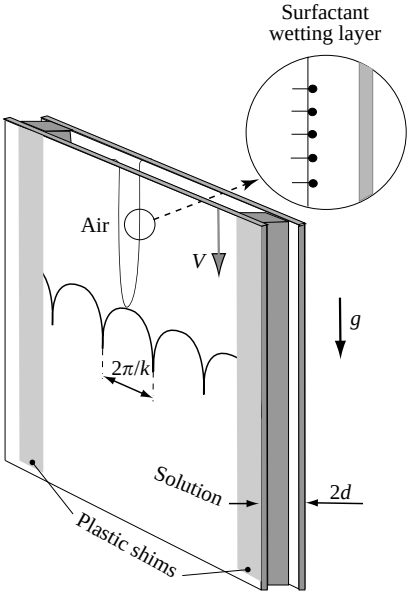


FIGURE 1. Schematic of the experimental setup.

| | | | | | | | | | | | |
|---|---|---|---|---|---|---|---|---|---|---|---|
| $c \times 10^{-3}$ (mol l$^{-1}$) | 2.4 | 2.8 | 3.3 | 4.0 | 4.6 | 5.2 | 5.8 | 7.0 | 7.8 | 8.0 | 8.3 |
| $c$/CMC | 0.28 | 0.33 | 0.38 | 0.46 | 0.53 | 0.63 | 0.67 | 0.81 | 0.93 | 0.96 | 1.00 |
| $\sigma_{eq}$ (dyn cm$^{-1}$) | 55 | 51 | 48 | 44 | 43 | 41 | 40 | 39 | 39 | 38 | 38 |

TABLE 1. SDS concentrations used in the experiments and the corresponding equilibrium surface tension $\sigma_{eq}$ measured by Tajima *et al.* (1970).

which, by the Landau–Levich law for dip-coating, results in film thicknesses on the order of 1 to 30 microns. After a short pause of 15 s (justified by the adsorption time, $t_a < 1$ s, as demonstrated in the next subsection) the cell is lowered with a constant dipping speed $V$ into the same surfactant solution. We do not expect any significant change in the film thickness during the short pause. The velocity of gravity drainage for such thin films is estimated to be of the order of $10^{-2}$ mm s$^{-1}$, and can be safely neglected. Furthermore, no significant evaporation is to be expected since the solutions are at room temperature. As a consequence of lowering the cell, the meniscus, when viewed in the reference frame of the plate, is driven toward the air. The location of the air/liquid interface is recorded from the side with a CCD camera (GL1 Canon) at 30 frames s$^{-1}$ with a spatial resolution of $2.2 \times 10^{-2}$ cm/pixel. This procedure is exactly the same one used by Chan & Liang (1997). After each experiment, the cell is disassembled and placed in a bath of acetone for 20 minutes. The plates are then rinsed with ethanol and then with deionized water. The cell is reassembled carefully, avoiding any contamination or deposition of dust on the surface plates.

In our experiments only a single-component surfactant of well-characterized kinetics is used. For this purpose, SDS, which is an anionic and soluble surfactant, with a 99% purity (Sigma-Aldrich), is best suited. The basic properties of SDS are reviewed in the next subsection. The experiments were performed with fresh solutions of SDS in deionized water at the bulk concentrations listed in table 1 (together with the corresponding equilibrium surface tension). The surface tension used to evaluate the

capillary number is the equilibrium value for the particular concentration. The viscosity of the different aqueous solutions is measured with a Cannon-Fenske viscometer with accuracy 0.5% and does not change with the SDS concentration; thus $\mu = 10^{-2}$ P is assumed. Although SDS is known to increase the wetting properties of water (cf. Rosen 1989), it proved necessary to treat the surface of the glass plates to obtain a uniform wetting layer, especially at low bulk concentrations. For this purpose, the plates were roughened with a fine 600-grit sandpaper (1 abrasive grain/42 μm). This treatment enhances the wetting properties of water on glass surfaces and in this way the plates could be coated with the SDS solution over the range of concentrations listed in table 1. We emphasize that having a roughened substrate is not crucially important for the instability to take place – the same patterns were observed for smooth substrates, but in view of the poor wetting properties in the low concentration range we do not report these measurements.

### 2.2. *Physical properties of SDS*

In this subsection we provide a concise summary of the equilibrium and non-equilibrium kinetic and material properties of SDS, which are necessary for estimates of characteristic times of the different processes involved and for our linear stability analysis in § 4, where we compare it with our experimental observations. To denote SDS concentration we will be using either capital $C$, which is always dimensional by the context, or lower-case $c$, which is non-dimensional and defined as $c = C/C_m$ with $C_m$ being the CMC concentration of 8.3 mM.

The surfactant (chemical formula $C_{12}H_{25}NaO_4S$) used in the experiments is of ionic type with molar mass of 288.380 g mole$^{-1}$. It should be mentioned that there is no agreement on values of key constants even for the equilibrium case: for example Fdhila & Duineveld (1996) state for the Langmuir constant:

$$K_L = \frac{k_a}{k_d \Gamma_m} = 13.0 \frac{\mathrm{m}^3}{\mathrm{mol}}, \text{ where } \Gamma_m = 10^{-5} \frac{\mathrm{mol}}{\mathrm{m}^2},$$

based on a least-square fitting to the data by Woolfrey, Banzon & Groves (1987). Several authors, e.g. Shen *et al.* (2002), use this value in their works. But the analysis by Chang, Wang & Franses (1992) of the data by Elworthy & Mysels (1966) gives the value

$$K_L = \frac{k_a}{k_d \Gamma_m} = 0.11 \frac{\mathrm{m}^3}{\mathrm{mol}}, \tag{2.1}$$

which is in the better agreement with equilibrium adsorption data and therefore is used in our calculations.

Equilibrium data for surface concentration $\Gamma$ *vs.* bulk concentration $C$ are given in figure 2($a$): the equilibrium adsorption plot demonstrates the applicability of the $K_L$ value in (2.1) versus that given by Fdhila & Duineveld (1996). The material behaviour of SDS, $\sigma(C)$, is given in figure 2($b$), where we compare the data by Tajima, Muramatsu & Sakaki (1970) (circles), measured by the drop volume method, predictions by Szyszkowsky equation (dashed curve):

$$\sigma^* = \sigma_0 + 2RT\Gamma_m \ln(1 + K_L C),$$

and least-square fitting of $\sigma^*$ with an additional polynomial to reflect the true behaviour at high concentrations (solid curve):

$$\sigma = \sigma_0 \{0.715(c - 2.745)(c - 0.519) + 1.76 \ln(1 + 0.91c)\}.$$

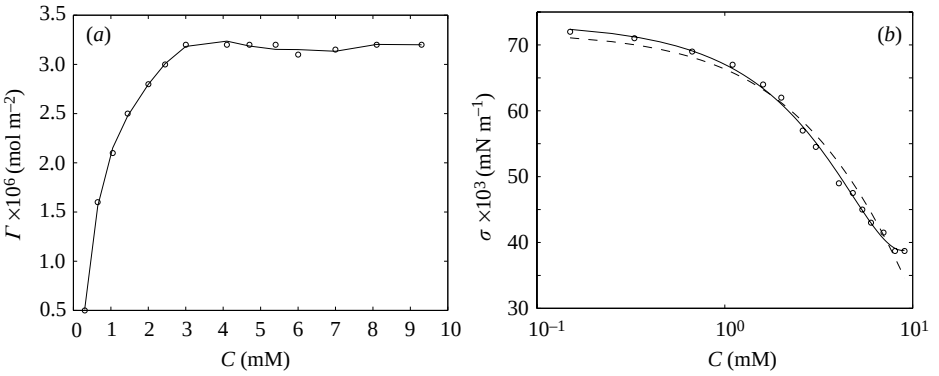


FIGURE 2. Equilibrium data for SDS. (*a*) Adsorption isotherm of SDS at air-solution interface at $T = 25\,^{\circ}$C. ○, data by Tajima *et al.* (1970); —, least square fitting. (*b*) Surface tension *vs.* bulk concentration of SDS solution: ○, data by Tajima *et al.* (1970); – –, Szyszkowski equation; —, least square fitting.

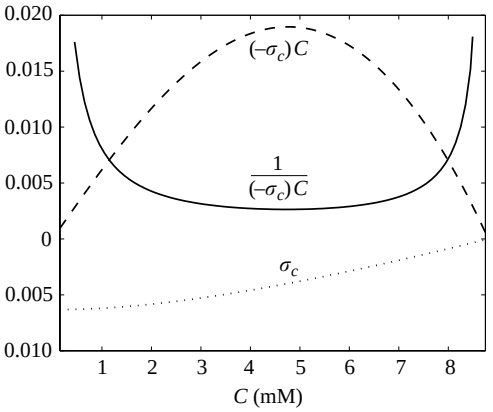


FIGURE 3. Material behaviour of SDS.

In our calculations, we use the last curve since it depicts the saturation phenomenon as opposed to the Szyszkowski equation. Figure 3 represents further information on the material behaviour of SDS: $\sigma_c$, which is a derivative of $\sigma(C)$ with respect to the argument, and $(-\sigma_c)C$, which will be used in our further discussion in §4. It must be noted that the experimental data in figure 2(*b*) indicate a change of second derivative sign, $\sigma_{cc}$, for concentrations between (2–5) mM, which substantially changes the material behaviour $\sigma_c$.

While there are some (scattered) data for equilibrium Langmuir kinetics, there are no available data for different bulk concentrations in the non-equilibrium case of Langmuir–Hinshelwood (L-H) kinetics:

$$\frac{\mathrm{d}\Gamma}{\mathrm{d}t} = k_a C(1-\theta) - k_d \Gamma,$$

where $\theta$ is a fractional coverage. Understanding L-H kinetic properties is of particular importance since it provides a relatively simple model and also allows us to evaluate different sorption characteristic times influencing the experimental procedure. However, Chang & Franses (1992) mention that this model does not provide a concise

| Concentration (mM) | Adsorption $k_a^*$ ($m\,s^{-1}$) | Desorption $k_d^*$ ($s^{-1}$) | Parameter $B$ |
|---|---|---|---|
| 1.7 | $5.5\times10^{-4}$ | 500 | 52 |
| 3.3 | $9.0\times10^{-4}$ | 818 | 22 |
| 5.9 | $2.8\times10^{-2}$ | $2.55\times10^{4}$ | 22 |
| 8.1 | 3.0 | $2.73\times10^{6}$ | 32 |

TABLE 2. Kinetics data for SDS at 25°C.

fit of the data and proposed a modified Langmuir–Hinshelwood (mL-H) equation

$$\frac{\mathrm{d}\Gamma}{\mathrm{d}t} = k_a^* C(1-\theta)\mathrm{e}^{-B\theta} - k_d^*\Gamma\mathrm{e}^{-B\theta},$$

which differs from L-H by the empirical constant $B$, amounting to an activation energy barrier concept. This model allows a better fit to the data, but at the expense of having all constants $k_a^*$, $k_d^*$ and $B$ as functions of the bulk concentration $C$, as indicated in table 2.

For our purposes we need just an approximate model of L-H type, which can be derived from the mL-H by conditional averaging, the essence of which consists in obtaining $k_a$ and $k_d$ by averaging over the bulk concentration:

$$k_a = \langle w k_a^* \mathrm{e}^{-B\theta}\rangle_C = \frac{1}{C_2-C_1}\int_{C_1}^{C_2} w(c)k_a^*(C)\,\mathrm{e}^{-B(C)\theta}\,\mathrm{d}C, \quad \min_w \int_{C_1}^{C_2}[w(C)-1]\,\mathrm{d}C,$$

such that equilibrium Langmuir constant $K_L$ is kept fixed. The weight $w(C)$ is equal to unity in our case (incidentally), but in general should be determined in the course of conditional averaging. The calculation gives

$$k_a = 0.64\times10^{-5}\,\frac{\mathrm{m}}{\mathrm{s}}, \qquad k_d = 5.87\,\mathrm{s}^{-1}.$$

This allows us to compare the characteristic times of different processes involved in our experiments:

(*a*) Residence time: since the working distance of the dipping process is $\sim 20$ cm and the speed of dipping $\sim 1\,\mathrm{cm\,s^{-1}}$, the characteristic time of the experiment is

$$t_{exp} \sim 20\,\mathrm{s}.$$

(*b*) Diffusion time: since mixing can take place only in the meniscus region of size $d \sim 300\,\mu\mathrm{m}$ and the diffusivity of SDS in water (estimated from limiting ionic mobilities) is $D = 8\times10^{-10}\,\mathrm{m^2\,s^{-1}}$, the diffusion characteristic time is

$$t_{diff} \sim \frac{d^2}{D} \simeq 10^2\,\mathrm{s}.$$

(*c*) Averaged time of adsorption:

$$t_a = \frac{\Gamma_m}{k_a C} < 1\,\mathrm{s},$$

for the working range of concentrations $C \in (1.5, 8.2)\,\mathrm{mM}$.

(*d*) Averaged time of desorption:

$$t_d = \frac{1}{k_d} < 0.2\,\mathrm{s}.$$

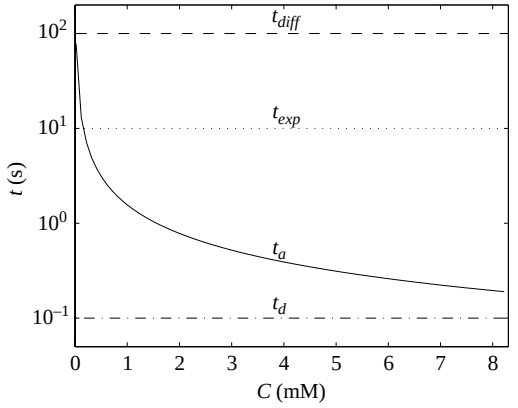


FIGURE 4. Separation of characteristic time scale.

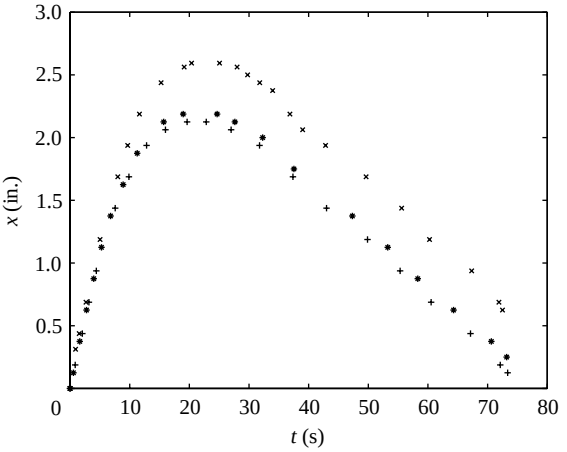


FIGURE 5. Interface position during withdrawal in the laboratory frame for concentrations $C = 2.4\,\mathrm{mM}$ (×), $C = 4.6\,\mathrm{mM}$ (●), $C = 5.8\,\mathrm{mM}$ (+).

Therefore, in view of the separation of time scales (cf. figure 4), the dynamics can be modelled by Langmuir–Hinshelwood kinetics.

## 3. Linear regime: critical conditions

Some preliminary experiments were performed to repeat the experiments of Chan & Liang (1997). We observed that there exists a critical speed above which the instability occurs and the fingering patterns are very similar to those in figure 2 of Chan & Liang (1997). Furthermore, we verified the crucial effect of surfactant and the wetting layer by performing the following experiments. In the first a wetting layer of pure water was deposited on the walls of the cell. When the cell was driven into the soap solution, no instability was observed for a wide range of dipping speeds. In the second experiment, the cell was coated with a wetting layer of surfactants solution and driven into pure deionized water. In this case, we observe the same fingering patterns. These two experiments show the importance of the presence of surfactants in the wetting layer in causing this instability.

Another effect revealed in our experiments can be seen from figure 5, where the position of the interface as a function of time in the laboratory frame is recorded. For

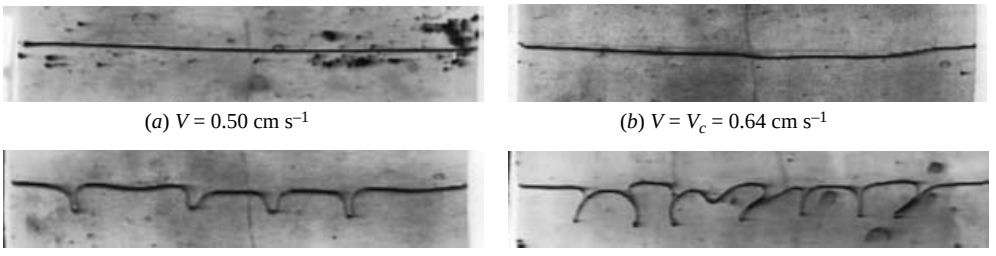

(*a*) $V = 0.50$ cm s$^{-1}$ (*b*) $V = V_c = 0.64$ cm s$^{-1}$

(*c*) $V = 1.52$ cm s$^{-1}$ (*d*) $V = 3.56$ cm s$^{-1}$

FIGURE 6. Typical fingering patterns for different dipping speeds. The width of the images is 10 cm.

times $t \in [0, 22]$ s the interface moves up along with the withdrawing cell (however with lower speed) since in this regime viscous friction dominates the hydrostatic pressure gradient. But upon reaching a certain height these two major forces interchange their roles. It is obvious that the speed of the interface relative the cell is different from that of withdrawal and this difference is a function of gravity, viscosity and the speed of withdrawal, with negligible dependence on the surface tension variation effects. The last fact follows from the local influence of the capillarity near the meniscus versus the global friction effect over the entire cell. Since the relationship between the actual speed of dip-coating and the speed of withdrawal is monotonic we use the latter as a working experimental variable.

### 3.1. *Determining criticality*

We show, in figure 6, typical images of the fingering patterns observed in the experiments for different dipping speeds $V$ for fixed bulk concentration, $c = 0.67$ CMC, and fixed withdrawal speed, $V_d = 2.03\,\mathrm{cm\,s^{-1}}$. We observe the existence of a threshold velocity. Below a critical speed $V_c$, the interface remains essentially flat (figure 6*a*): as the dipping speed increases, the interface develops fingering patterns with different amplitudes. As in all such experiments the critical condition is difficult to measure accurately, since it depends on determining weak growth or decay of nearly neutral modes during a finite duration experiment. Furthermore, the instability is typically very long wavelength, making the determination of $V_c$ somewhat subjective, since it is difficult to distinguish between a long-wave instability and finite domain effects. Nonetheless, we can bracket the critical speed to within 4%. Figure 6(*b*) shows a slightly deformed interface for a dipping speed equal to the critical velocity $V_c$. Figure 6(*c*) shows the fingering patterns for a dipping speed $V$ approximately twice $V_c$ where the fingers are non-uniformly spaced at the interface. The waveform typically consists of a blunted front and sharp trailing tail. At higher dipping speeds ($V \sim 5V_c$), figure 6(*d*), the fingers show very nonlinear dynamics which we discuss in § 5.

### 3.2. *Critical velocity $V_c$*

The instability was studied for the different concentrations of SDS listed in table 1. Over 100 experiments were performed for a wide range of withdrawal speed (and thus film thickness) and for dipping speeds $V$ from 0.127 to $3.56\,\mathrm{cm\,s^{-1}}$. Figure 7 shows the measurements of $V_c$ versus the SDS concentration for different withdrawal speeds. The qualitative behaviour of the critical velocity with $C$ is the same for all fixed withdrawal speeds. For very low concentrations, $c < 0.2$, no instability occurs: the air/liquid interface remains flat, even at the highest dipping speed which can

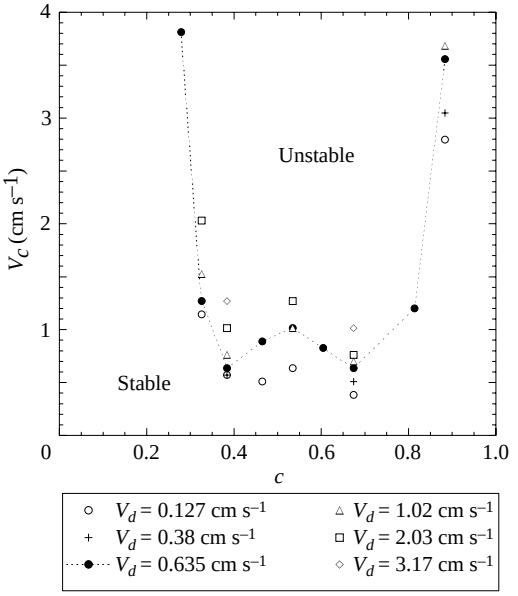


FIGURE 7. $V_c$ versus $c$/CMC. No instability occurs above CMC.

be attained in our facilities. As the concentration increases, $V_c$ drops to a first local minimum at $c \sim 0.33$. In the intermediate range of concentration, $0.33 < c < 0.7$, the critical velocity increases again and decreases to a second local minimum at $c = 0.7$. For higher concentrations, $c \geqslant 0.8$, the critical velocity increases quickly. This is a striking observation and in disagreement with the experimental results of Chan & Liang (1997), but confirms the theoretical prediction by Krechetnikov & Homsy (2004). Chan & Liang (1997) observe that with SDS, the concentration should be above CMC, and to produce the instability clearly and reproducibly they used $c = 4$ and measure a critical velocity of $1.9\,\mathrm{cm\,s^{-1}}$. We repeated several experiments at $c = 2$ and $c = 4$ without observing any instability. Moreover if the interface is perturbed by some drops falling into the solution, the air/liquid interface still remains flat. The difference between our observations and those from Chan & Liang (1997) can perhaps be explained by the fact that SDS used by Chan & Liang (1997) does not have the same purity as that used in our experiments. Lastly, figure 7 suggests a weak dependence of $V_c$ on $V_d$: the increase in withdrawal speed $V_d$ leads to an increase in the critical speed $V_c$ for a given concentration. As we will see in § 4.4, this behaviour is consistent with thickening of the wetting layer, which grows like $Ca_d^{2/3}$ according to Landau–Levich theory.

## 4. Comparison with linear theory

While the detailed theory is developed in Krechetnikov & Homsy (2004), here we provide its basic formulation in the low capillary, $Ca = \mu V/\sigma$, and Bond, $Bo = \rho g d^2/\sigma$, number regime. The problem is considered in a Cartesian system of coordinates (refer to figure 8). For coordinates we use $(x, y, z)$ as shown in figure 8, with corresponding velocities $(u, v, w)$. We neglect the gas-phase dynamics and formulate the equations in the one-fluid approximation. Also, the surfactant exchange between bulk and interface is modelled by sorption kinetics, which is the principal mode of the

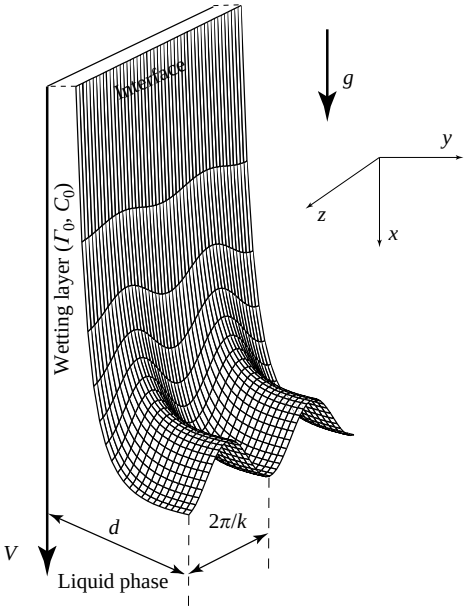


FIGURE 8. Basic setup.

surfactant transport (justified by the large value of Péclet number), so that surfactant interchange between surface and bulk is kinetically controlled. Therefore, we do not need to consider the bulk concentration dynamics. The general problem contains the following independent physical parameters: surfactant concentrations in the wetting layer $C_0, \Gamma_0$; two kinetic parameters $k_a, k_d$ – the rates of adsorption and desorption respectively; two geometrical parameters $(d, \overline{h}_\infty)$; the plate speed $V$ and speed of withdrawing $V_d$; the external field of gravity $g$; and three material properties of the liquid $(\rho, \sigma, \mu)$.

Since $Bo \sim 10^{-2}$ throughout all experiments, the appropriate length scale is half the gap width rather than the capillary length, so that the $y$-coordinate is scaled with respect to the thickness of a gravity-free film deposited by withdrawing the cell with speed $V_d$:

$$\overline{h}_\infty \sim d\left(\frac{\mu V_d}{\sigma}\right)^{2/3} \equiv d\, Ca_d^{2/3},$$

that is $\overline{y} = dy$, $\overline{h} = dh$ with the further non-dimensional scaling:

$$y = -1 + Ca_d^{2/3}\,\widehat{y}, \quad h = 1 - Ca_d^{2/3}\widehat{h}.$$

The form of the latter is given for the branch $y = -h(t, x, z)$ of the interface. The general problem statement suggests the standard non-dimensionalizations for time and space coordinates $\overline{t} = (d/v)t$, $\overline{x} = dx$, $\overline{z} = dz$, pressure $\overline{p} = (\sigma_0/d)p$, and the two stream functions (required to describe a three-dimensional flow such that $u = \psi_y$, $w = \phi_y$, $v = -\psi_x - \phi_z$), $\overline{\psi} = (V/d)\psi$, $\overline{\varphi} = (V/d)\varphi$. Following the procedure of Park & Homsy (1984), the importance of axial pressure gradients and the viscous terms (in view of no-slip boundary condition at the wall) dictates the scalings

$$t = \frac{Ca_d^{4/3}}{Ca}\,\widehat{t},\; x = \frac{Ca_d^{4/3}}{Ca}\,\widehat{x},\; z = \frac{Ca_d^{4/3}}{Ca}\,\widehat{z}; \quad p = \widehat{p},\; \psi = Ca_d^{2/3}\widehat{\psi},\; \varphi = Ca_d^{2/3}\widehat{\varphi},$$

where $Ca_d^{4/3}/Ca$ comes from the presence of the two independent capillary numbers, $Ca_d$ (withdrawing) and $Ca$ (dipping). When $Ca_d = Ca$, one recovers the classical scaling $Ca^{1/3}$. The material properties (interfacial tension and surfactant concentration) are scaled with respect to the appropriate values in the pre-existing wetting layer,

$$\overline{\sigma} = \sigma_0(\Gamma_0)\,\sigma,\ \overline{\gamma} = \Gamma_0\,\gamma.$$

Further we use capitals for the basic-state variables and lower case for disturbance variables.

As demonstrated in Krechetnikov & Homsy (2004), the observed instability is due to significant surface tension gradients. Here we split the analysis in two basic steps: first we recapitulate the demonstration of Krechetnikov & Homsy (2004) of the intrinsic instability of an interface under the presence of surface concentration gradients and then we study the formation of this gradient in our particular situation.

### 4.1. *Linearized stability equations*

Consideration of the temporal stability of the parallel ($x$-independent) basic state

$$\widehat{H} = \text{const},\ \widehat{P} = 0,\ \Sigma = \text{const},\ \widehat{\Gamma} = \text{const},\ \widehat{U} = 1,\ \widehat{V} = \widehat{W} = 0,$$

leads to the following set of linear disturbance equations (with $\Delta$ being the in-plane Laplacian, $\partial_x^2 + \partial_z^2$):

velocity field,

$$\widehat{\psi}'_{yyy} = \widehat{p}'_x,$$
$$\widehat{\varphi}'_{yyy} = \widehat{p}'_z,$$

surfactant transport,

$$\widehat{\gamma}'_t + \widehat{\Gamma}(\widehat{\psi}'_{xy} + \widehat{\varphi}'_{yz}) + \widehat{\Psi}_y\gamma'_x = \frac{Ca}{Ca_d^{4/3}}\frac{1}{Pe_s}\Delta\widehat{\gamma}' - \frac{Ca_d^{4/3}}{Ca}\kappa St[K\rho + 1]\widehat{\gamma}',$$

interfacial conditions:

kinematic,

$$\widehat{h}'_t + \widehat{\Psi}_y\widehat{h}'_x = -\widehat{\psi}'_x - \widehat{\varphi}'_z,$$

normal dynamic,

$$\widehat{p}' + \left(\frac{Ca}{Ca_d}\right)^2 \Sigma\Delta\widehat{h}' = -2\left(\frac{Ca}{Ca_d}\right)^2 Ca_d^{2/3}[\widehat{\psi}'_{xy} + \widehat{\varphi}'_{yz}],$$

tangential dynamic,

$$\Sigma_\Gamma\widehat{\gamma}'_x = Ca_d^{2/3}\widehat{\psi}'_{yy},$$
$$\Sigma_\Gamma\widehat{\gamma}'_z = Ca_d^{2/3}\widehat{\varphi}'_{yy},$$

and no-slip boundary conditions at the wall,

$$\widehat{y} = 0\text{:}\ \widehat{\psi}' = \widehat{\psi}'_y = 0,\quad \widehat{\varphi}' = \widehat{\varphi}'_y = 0.$$

The several non-dimensional parameters are given by

$$Ca = \frac{\mu V}{\sigma_0},\quad Ca_d = \frac{\mu V_d}{\sigma_0},\quad St = \frac{k_a}{V},\quad K = \frac{k_a C_0}{k_d\Gamma_0},\quad \kappa = \frac{d\,C_0}{\Gamma_0}\frac{1}{K},\quad \rho = \frac{\Gamma_0}{\Gamma_m}.$$

Eliminating the disturbance pressure and velocity field, and transforming the result to Fourier space the final system for linear evolution of disturbances can be cast in the canonical form:

$$\widetilde{\gamma}_t' + a\widetilde{\gamma}_x' + \underset{\text{III}}{\widetilde{\gamma}} - (\underset{\text{V}}{\zeta m} + \underset{\text{II}}{\eta})\Delta\widetilde{\gamma} = -\frac{3}{2}\left[\underset{\text{I}}{\Delta^2}\widetilde{h} - m\underset{\text{IV}}{\Delta^2}\widetilde{\gamma}\right], \tag{4.1a}$$

$$\widetilde{h}_t' + a\widetilde{h}_x' = -\left[\underset{\text{I}}{\Delta^2}\widetilde{h} - m\underset{\text{IV}}{\Delta^2}\widetilde{\gamma}\right] + \frac{\zeta m}{2}\underset{\text{V}}{\Delta}\widetilde{\gamma}. \tag{4.1b}$$

Here we utilized the definitions:

$$m = -2\frac{\Gamma\Sigma_\Gamma}{\Sigma}, \quad \zeta = \frac{1}{2}\frac{1}{Ca_d^{1/3}}\left(\frac{3\Sigma}{\widehat{H}\kappa\, St\, Ca\,(K\rho+1)}\right)^{1/2}, \quad \eta = \frac{\tau}{\xi^2}\frac{Ca}{Ca_d^{4/3}}\frac{1}{Pe_s}, \quad a = \frac{\tau}{\xi},$$

where the parameter $m$ is a primary bifurcation parameter containing the physics of the surfactant material behaviour.

The physical meaning and origin of each term in these equation are discussed in detail by Krechetnikov & Homsy (2004). Here we just note from (4.1$a$) that the effects of surface tension (capillary pressure$^{(\text{I})}$), surface diffusion$^{(\text{II})}$ and bulk-interface interchange$^{(\text{III})}$ ($St > 0$) are stabilizing, while the effect of the Marangoni stresses$^{(\text{IV})}$, ($\Sigma_\Gamma < 0$), is destabilizing as it comes from the normal dynamical condition. At the same time, the Marangoni effect$^{(\text{V})}$, originating from the advection of surfactant by the Marangoni-induced disturbance flow, is stabilizing. As we will see from the normal-mode analysis the destabilizing Marangoni stresses overcome the stabilizing role of the other contributions and produces the instability.

### 4.2. *Normal-mode analysis*

Assuming the normal mode of the disturbance to be of the form

$$\begin{pmatrix}\widetilde{\gamma}\\ \widetilde{h}\end{pmatrix} = \mathrm{e}^{\lambda t + \mathrm{i}kz + \varepsilon x}\begin{pmatrix}\bar{\gamma}\\ \bar{h}\end{pmatrix}, \quad \mathrm{Re}(\varepsilon) > 0,$$

where $\varepsilon$ is the rate of the disturbance decay as $\widetilde{x} \to -\infty$, we find that the dispersion relation is a function of the scaled wavenumber $k$, the material behaviour $m$, sorption–desorption kinetics $\zeta$ and the surface diffusion $\eta$:

$$\lambda^2 + b\lambda + c = 0, \tag{4.2}$$

with

$$b = 2a\varepsilon + 1 + \left(1 - \tfrac{3}{2}m\right)\delta^2 + (\zeta m + \eta)\delta,$$
$$c = (a\varepsilon + \delta^2)\left(1 + a\varepsilon + \delta(\zeta m + \eta) - \tfrac{3}{2}m\delta^2\right) - \tfrac{3}{2}m\delta^2\left(\tfrac{1}{2}\zeta\delta - \delta^2\right),$$

where $\delta = k^2 - \varepsilon^2$. In the presence of surfactants the largest growth rate corresponds to zero wavenumber (in reality there is a cut-off due to the finite cell width)

$$\lambda = -2(1 - m\varepsilon^2\zeta) + O(\varepsilon),$$

so that the critical bifurcation parameter corresponds to

$$m \sim \frac{1}{\zeta\varepsilon^2} \Longleftrightarrow -2\frac{\Gamma\Sigma_\Gamma}{\Sigma} \sim \frac{2Ca_d^{1/3}}{\varepsilon^2}\left(\frac{H\kappa St\, Ca\,(K\rho+1)}{3\Sigma}\right)^{1/2}. \tag{4.3}$$

As discussed in detail below, equation (4.3) connects the critical speed to the key kinetic and material parameters and to the wetting film thickness. The instability can

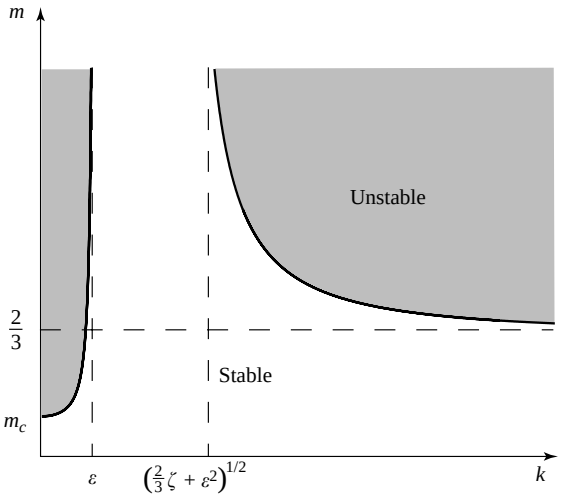


FIGURE 9. Locus of $\mathrm{Re}(\lambda_1) = 0$. The bold curves correspond to the marginal stability conditions. The flow is unstable above and stable below these curves.

be understood as the effect of thickening of the transition region – the growth of the $v$ component of the disturbance velocity. It should be noticed from (4.3) that the dependence for the bifurcation parameter

$$m \sim \widehat{H}^{1/2},$$

has non-trivial physical consequences, as will be discussed later. Thus, the global bifurcation point is given by

$$\left(k_c = 0, \quad m_c = \frac{1}{\zeta \varepsilon^2}\right).$$

The locus of $\mathrm{Re}(\lambda_1) = 0$ for the most unstable eigenvalue $\lambda_1$ in the case $\zeta \gg 1$, $\varepsilon \ll 1$, $\eta \ll 1$ is depicted in figure 9 as a bold curve and essentially means that for any $m > m_c$ there exist wavenumbers $k$ near the origin such that the instability takes place.

### 4.3. *Surfactant accumulation in a cap region*

As one can infer from (4.3), there is no dependence of $m_c$ on the speed of dipping since *Ca St* is independent of $V$: the above analysis corresponds to the intrinsic instability of the interface, which does not 'know' anything about its motion. Of course, a true free film does not exhibit instability in view of the homogeneous distribution of surfactant in a state of equilibrium. Thus, the instability appears only under conditions favourable to the creation of significant gradients in surfactant concentration. The problem considered here is one those cases: the effect of accumulation of the surfactant in a cap region due to the motion of the plates is a mechanism by which the required concentration gradients are produced.

In order to connect the intrinsic instability of a thin film with the effect of accumulation, one needs to use the appropriate expression for the surfactant concentration $\Gamma$. From a simple balance of surfactant transport in a cap region (cf. figure 10) we have

$$-2\Gamma_0 V = l[k_a C_0(1 - \rho\Gamma) - k_d \Gamma_0 \Gamma],$$

with $l$ being the effective length of the interface, where equilibrated exchange with the bulk takes place (taken as the meniscus length, $l \simeq \pi d$). Thus the effect of accumulation

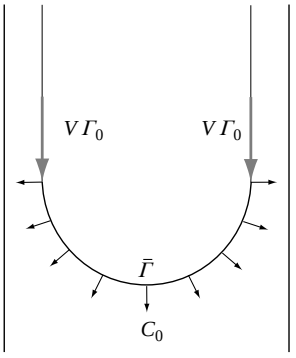


FIGURE 10. Surfactant transport in a cap region.

results in the concentration in the cap region

$$\Gamma = \frac{1 + 2(d/l)/St\kappa'}{\rho(1 + 1/\rho K)}, \text{ with } \kappa' = \frac{dC_0}{\Gamma_0}, \tag{4.4}$$

which is higher than that in the wetting layer and entails the existence of a surfactant concentration gradient. This linear approximation does not account for either nonlinear or saturation phenomenon, but nevertheless is valid for a wide range of speeds since $V \ll d\,k_d$ in most cases.

### 4.4. *Prediction of critical functionality*

Using (4.4), (4.3) can be simplified to give an expression for the dimensionless critical speed

$$\frac{V_c}{lk_d} = \frac{1 + K_m c}{2}\left(A\frac{\sigma^{1/2}}{(-\sigma_c)}\frac{\widehat{H}^{1/2}}{c(1 + K_m c)^{1/2}} - 1\right), \quad A = \left(\frac{Ca\,St\,\kappa}{3}\right)^{1/2}\frac{Ca_d^{1/3}}{\varepsilon^2}, \tag{4.5}$$

where $K_m = k_a C_m / k_d \Gamma_m$, $\sigma$ is considered a function of $c$ and $\sigma_c$ as before is a derivative with respect to the argument. Thus, as follows from (4.5), the most important experimental quantities for a given surfactant are concentration, $c$ ($\equiv C_0/C_m$), and wetting layer thickness, $\widehat{H}$, which is considered as independent in view of its dependence on the speed of withdrawal $V_d$ through Marangoni effects. Therefore, the critical velocity $V_c$ can be considered as a function of these two parameters. Using typical material behaviour of pure surfactants $\sigma(c)$, as shown schematically in figure 3, the critical speed ratio $v_c$ as a function of the bulk concentration $c$ in a pre-existing wetting layer has the generic behaviour sketched in figure 11 when $\widehat{H}$ is taken to be independent of surfactant concentration. The first asymptote corresponds to the limit $c \to 0$, while the second one is associated with the saturation phenomenon close to CMC.

One of the governing experimental parameters is the dimensionless wetting layer thickness $\widehat{H}$, as suggested by the theory above. In our experiments, the coating process is characterized by low capillary numbers $Ca_d = \mu V_d/\sigma_{eq}$ in the range from $10^{-5}$ to $10^{-3}$ which, for our gap width, would result in wetting layer thicknesses from 1 to 30 microns according to the theory by Landau & Levich (1942). This order of magnitude of the film thickness is not substantially modified by the presence of a roughened substrate or a surfactant, which actually stabilize the film against the gravity drainage and dewetting instabilities. However there exist neither theory nor experimental studies of dip coating under these conditions. Therefore we discuss only

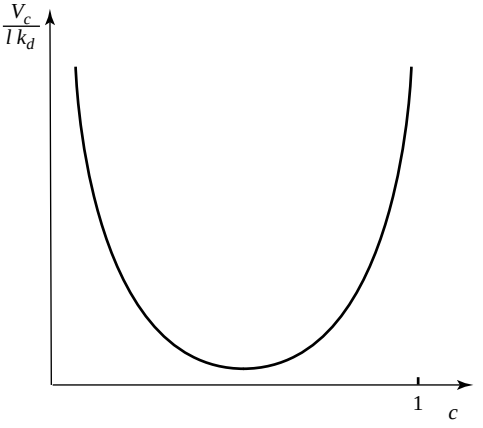


FIGURE 11. Generic marginal stability curve with $\widehat{H} = \text{const}$.

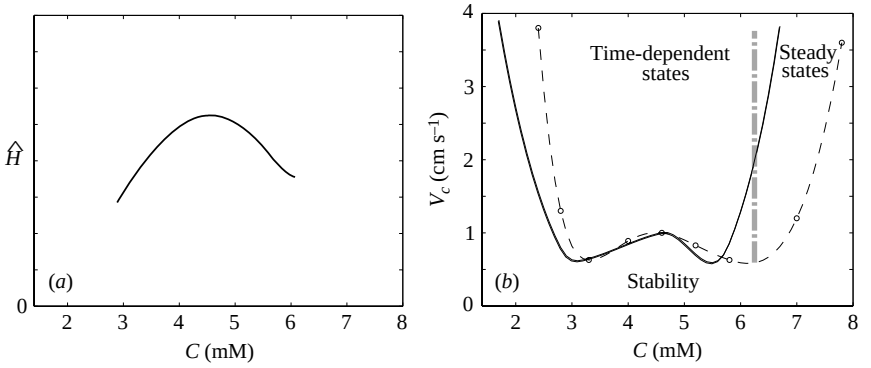


FIGURE 12. Marginal stability phenomenon: theory and experiment. (*a*) Schematic of wetting layer thickness $\widehat{H}$ as a function of surfactant concentration after Quéré (1999). (*b*) Comparison of the linear theory (solid curve) with $\widehat{H}$ from (*a*) and experimental data (dashed curve), $V = 0.64\,\text{cm s}^{-1}$.

a qualitative behaviour of the film thickness as shown in figure 12(*a*). This generic behaviour is analogous to that from the experimental study by de Ryck & Quéré (1993) (see also discussion in Quéré 1999), who measured film thickness for coating of a nickel wire with an SDS solution. Since the Bond number associated with the estimated roughness is much less than unity, one can expect smooth coating and therefore their setup is applicable. The maximum in the wetting film thickness is correlated with the inflection point in figure 3, at which, as speculated by Quéré (1999), the Marangoni flow is most efficient. However, we should note that there exists neither theoretical nor experimental confirmation of this predominant role of Marangoni effects.

Considering the constants $A$ and $l$ as empirical parameters (since their values can be established only from nonlinear analysis) and assuming the qualitative behaviour of $\widehat{H}$ depicted in figure 12(*a*), one can easily fit the curve to the experimental data as shown on figure 12(*b*). The hump present in the curve $V_c(c)$ (cf. figure 12*b*) for intermediate values of $c$ is due to the factor of $\widehat{H}^{1/2}$ in equation (4.5), whose functional dependence on $c$ is discussed above.

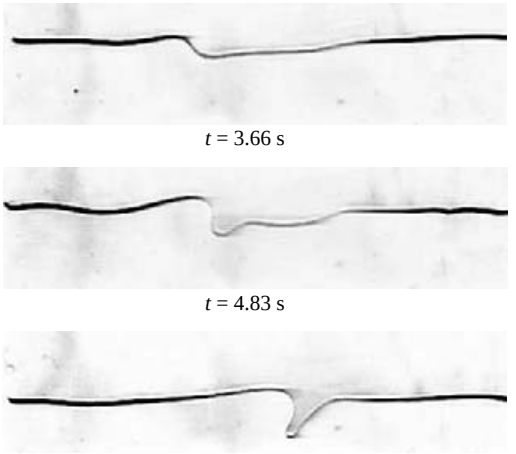


FIGURE 13. Drifting phenomenon – finger moving along the interface.

Concluding, we note that the experiments performed near the threshold of instability confirm well the theoretical predictions: namely, the generic shape of the marginal stability curve along with more subtle features such as a 'hump' for intermediate values of concentration. Finally, the primary discrepancy with the results by Chan & Liang (1997) – no instability above CMC – is validated experimentally.

## 5. Nonlinear regime

In this section, we present different regimes of pattern dynamics observed above the threshold of instability. We observe two different regimes, one in which the patterns are time-dependent and a second one in which they reach a steady state. In figure 12(*b*) the border between time-dependent and steady regimes of fingering is designated by a vertical line. In general, the time-dependent regime is more often observed, in which the fingers show a wide range of dynamics like drifting, merging of fingers and air bubble ejection, all of which are discussed below.

### 5.1. *Unsteady patterns: qualitative map*

*Drifting fingers* appear throughout the time-dependent unstable regime. Figure 13 shows images of a finger travelling along the interface for a surfactant solution of $C = 2.8 \times 10^{-3}\,\mathrm{mol\,l^{-1}}$, a dipping speed $V = 1.52\,\mathrm{cm\,s^{-1}}$, $(V/V_c = 1.1)$, and a withdrawal speed $V_d = 0.635\,\mathrm{cm\,s^{-1}}$. The finger grows near one boundary and travels from one side of the channel to the other at a constant speed $u$.

The second phenomenon in the time-dependent unstable regime is the *merging of fingers*. Figure 14 shows the evolution of the interface deformation when two fingers near the right boundary are merging together. As the fingers get closer together, the interface which separates them, initially flat, is distorted until the merging point. After this transition, the merged finger advances and ejects a small air bubble from the tail, which is the third phenomenon we observed.

*Cusp formation and bubble ejection* tend to occur at higher speeds, $V/V_c > 2$. Figure 15 shows the formation of air bubbles, which are ejected from the finger tails. We observe this process quite often and the images of figure 15 are taken from a series of experiments performed with a surfactant solution $c = 0.34$ and a fixed

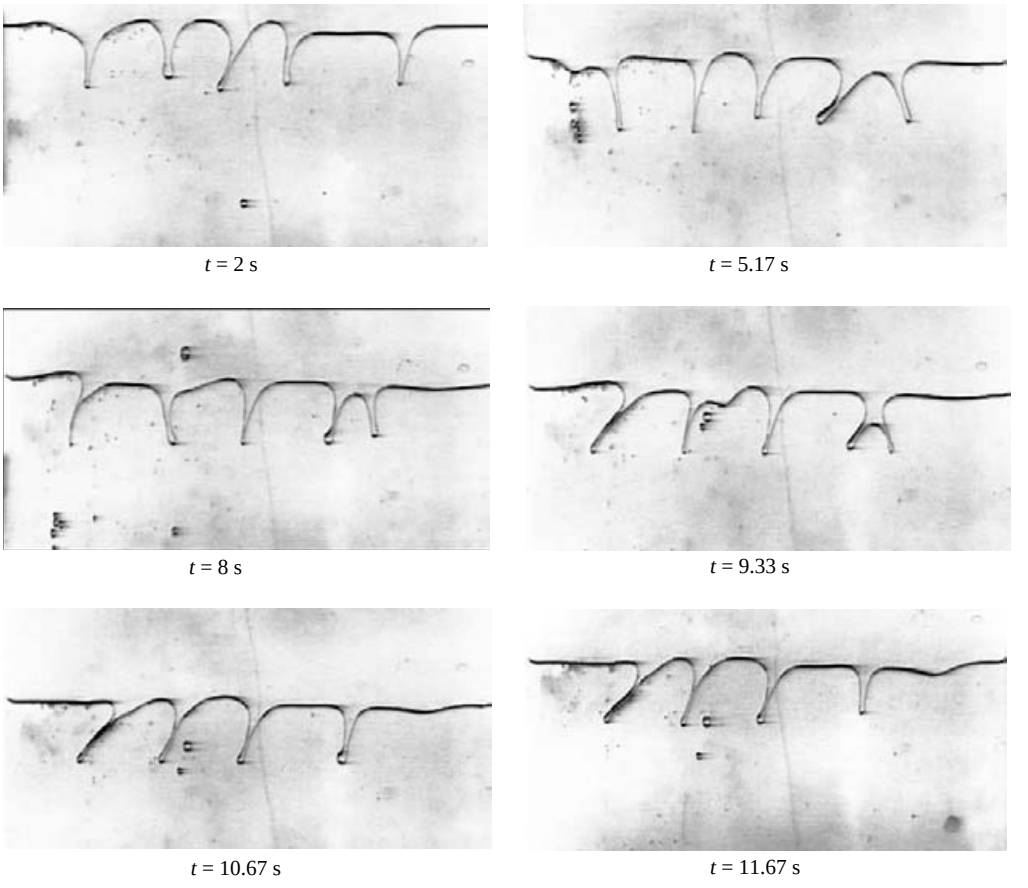


FIGURE 14. Merging phenomenon for a surfactant solution $c = 0.67$. The dipping speed is $V = 1.65\,\mathrm{cm\,s^{-1}}$ $(V/V_c = 2.4)$.

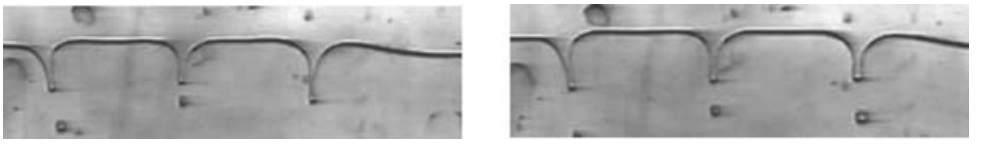

FIGURE 15. Bubble ejection phenomenon for a surfactant solution $c = 0.34$ (time runs from left to right). The dipping speed is $V = 3.3\,\mathrm{cm\,s^{-1}}$ $(V/V_c = 2)$.

withdrawal speed, $V_d = 1.02\,\mathrm{cm\,s^{-1}}$. Spatio-temporal diagrams (not shown) indicate that the phenomenon repeats itself in quasi-periodic fashion.

### 5.2. *Steady patterns*

A steady-state regime exists for a bulk concentrations $c \geqslant 0.67$ and for high withdrawal speeds, as shown in figure 16. For dipping speeds $V \geqslant 2.5V_c$, the finger shapes in the steady regime are similar. The interface advances at constant velocity and develops fingering patterns with blunt tips and sharp thin tails.

Figure 16 shows images of the evolution of the interface to a steady state for a bulk concentration $c = 0.67$ and a dipping speed $V/V_c = 3.5$. At the beginning of the experiment, when the wetted cell is lowered into the surfactant solution, the interface

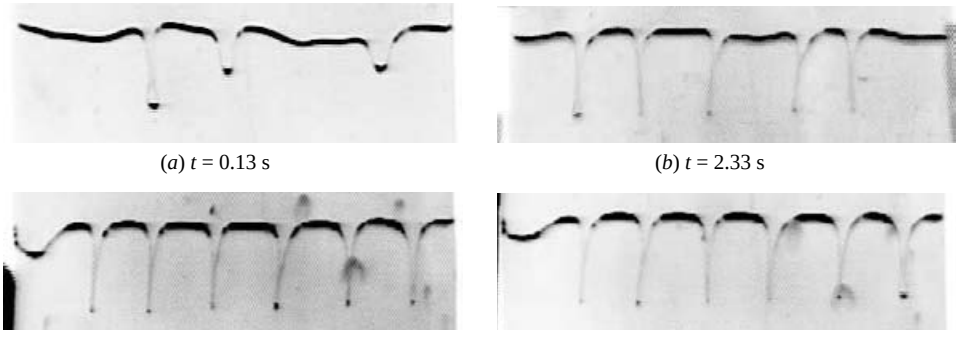


FIGURE 16. Evolution to a steady-state regime for bulk concentration of $c = 0.67$ and withdrawal speed $V_d = 2.03\,\mathrm{cm\,s^{-1}}$. The image width is 10 cm.

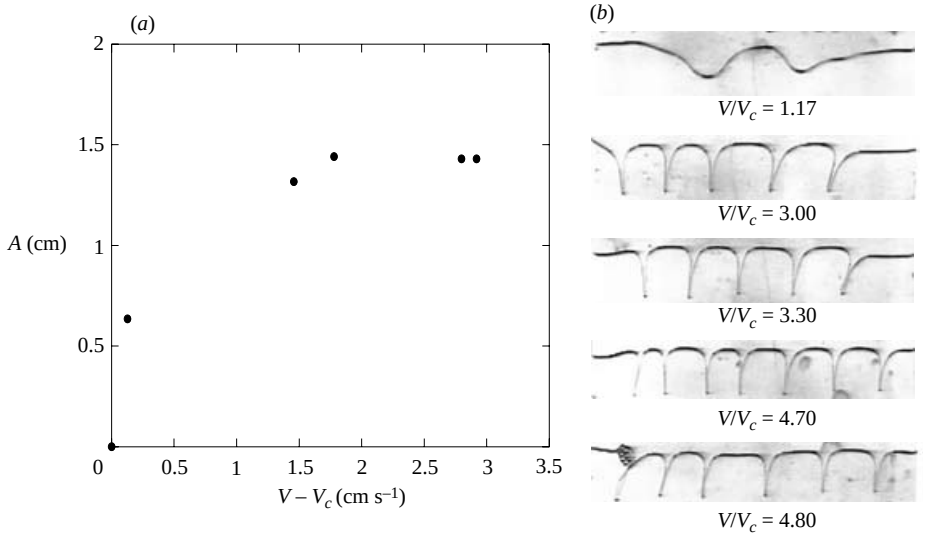


FIGURE 17. Amplitude of fingers for $c = 0.67$ and $V_c = 0.78\,\mathrm{cm\,s^{-1}}$. (*a*) Amplitude versus $V - V_c$. (*b*) Steady patterns.

remains flat for approximatively 2, after which it becomes unstable and perturbations start to grow. This deviation corresponds to the onset of the instability. After a transient, the interface evolves to a static periodic shape of constant wavelength. In the steady state, (figure 16*c*) flat regions of the interface move in the direction of the interface motion and sharp tails point in the opposite direction.

In figure 17 the amplitude of the fingers for the same surfactant solution $c = 0.67$ and fixed withdrawal speed is presented as a function of $V - V_c$. The measurements correspond to the average over all the steady patterns observed. For dipping speeds slightly above the critical velocity, the measurements are difficult because the cell reaches the bottom of the tank before the patterns are near a steady regime. Nevertheless, we find that the amplitude of the steady patterns increases as the dipping speed increases above the threshold until it reaches a plateau for speeds $V \geqslant 3V_c$. Although the data are sparse, this behaviour is suggestive of a supercritical bifurcation.

### 5.3. *Discussion*

Although we do not attempt a theoretical understanding of the various nonlinear phenomenon observed here, we do offer a few comments about them. The first obvious nonlinear feature is the limit to the depth of propagation of the fingers, independent of whether they equilibrate to steady structures or not. This is in contrast to viscous fingering in Hele-Shaw cells in which fingers propagate without limit. Furthermore, the wave form of the fingers is nearly harmonic at the critical condition and becomes increasingly complex in the nonlinear regime. These features – a limit to propagation and increasingly nonlinear wave forms leading to blunt fronts and sharp trailing troughs – are strikingly similar to other interfacial instability problems, notably directional solidification (cf. de Cheveigne, Guthmann & Lebrun 1986) and the ribbing instability (also referred to as the 'printer's instability'; cf. Rabaud 1994). In those problems, finger propagation is limited due to the presence of a stabilizing gradient in composition/temperature and capillary pressure, respectively. Such a stabilizing gradient is not present in the base state here, but may result from the complicated processes determining the surfactant distribution in both the axial direction and in the thin gap of the Hele-Shaw cell.

The other nonlinear phenomenon of drifting and merging are also qualitatively similar to those occurring in ribbing and directional solidification. In all these problems, the eigenvalues are not necessarily real as well, which means that standing waves are susceptible to symmetry-breaking secondary instabilities leading to drifting and merging. The origins of such secondary instabilities are myriad, but in the present experiments might be nucleated by inevitable non-uniformities in the wetting layer thickness, surface roughness, and/or the small gravity-driven drainage. We speculate that these mechanisms can appear at lower surfactant concentrations where they can compete more effectively with Marangoni stresses, which might explain the occurrence of steady patterns only for the higher concentrations of SDS.

Finally, the phenomenon of bubble ejection is reminiscent of similar features in ribbing, tip-streaming from drops (e.g. Taylor 1934), and cusp formation in surfactant solutions (e.g. Antanovskii 1994). All of these in turn are due to the local extensional flow, viewed in the frame of the fingers, being so strong as to overwhelm the capillary pressures due to surface tension and curvature in the sharp trailing regions of the fingers. In all these problems bubble ejection, tip-streaming and cusp formation occur when a suitably defined capillary number based on the local extension rate exceeds a critical value. This is consistent with our observation of bubble ejection only at high speeds.

The study of all these mechanisms and questions would involve detailed modelling of the flow and surfactant transport, coupled with nonlinear treatments of the free boundary problem, and is outside the scope of this paper.

## 6. Summary and conclusions

This experimental study has deepened our understanding of the simple, but fundamentally important, fingering phenomenon which is solely due to surfactant-driven surface tension variation effects.

We have clarified the effects of material behaviour and kinetic properties, in accord with the theoretical study of Krechetnikov & Homsy (2004), and a reasonable qualitative agreement was found with a linear theory. Notably, our experiments verify the theoretical prediction that no instability occurs above CMC, which provides support for the generic mechanism identified in Krechetnikov & Homsy (2004).

However, for an accurate quantitative comparison some further improvements of both theory and experiment are needed. In particular, measurements of wetting layer thickness as a function of surfactant concentration and substrate roughness are necessary. At the same time, the linear theory should be generalized to account for non-parallel effects along with a more accurate description of kinetic properties. Nevertheless, despite these shortcomings, a significant understanding of the underlying physics is attained.

A rich variety of nonlinear phenomenon is observed in this classical Hele-Shaw setup, which include unsteady merging and drifting of fingers, cusp formation with air bubble ejection, and steady fingering occurring over a narrow range of concentrations. All of these observed phenomenon lack any kind of theoretical description.

This work was supported by the Office of Basic Energy Sciences, US Department of Energy.

## REFERENCES

Antanovskii, L. K. 1994 Influence of surfactants on a creeping free-boundary flow induced by two counter-rotating horizontal thin cylnders. *Eur. J. Mech.* B **13**, 73–92.

Chan, C. K. 2000 Surfactant wetting layer driven instability in a Hele-Shaw cell. *Physica* A **288**, 315–325.

Chan, C. K. & Liang, N. Y. 1997 Observations of surfactant driven instability in a Hele-Shaw cell. *Phys. Rev. Lett*. **79**, 4381–4384.

Chang, C.-H. & Franses, E. I. 1992 Modified Langmuir-Hinshelwood kinetics for dynamic adsorption surfactants at the air/water interface. *Colloids Surfaces* **69**, 189–201.

Chang, C.-H., Wang, N.-H. L. & Franses, E. I. 1992 Adsorption dynamics of single and binary surfactants at the air/water interface. *Colloids Surfaces* **62**, 321–332.

de Cheveigne, S., Guthmann, C. & Lebrun, M. M. 1986 Cellular instabilities in directional solidification. *J. Phys. (Paris)* **47**, 2095–2103.

Elworthy, P. H. & Mysels, K. J. 1966 The surface tension of sodium dodecylsulfate solutions and the phase separation model of micelle formation. *J. Colloid Interface Sci.* **21**, 331–347.

Fdhila, R. B. & Duineveld, P. C. 1996 The effect of surfactant on the rise of a spherical bubble at high reynolds and peclet numbers. *Phys. Fluids* **8**, 310–321.

Krechetnikov, R. & Homsy, G. M. 2004 On new surfactant-driven fingering phenomenon in a Hele-Shaw cell. *J. Fluid Mech.* **509**, 103–124.

Landau, L. & Levich, B. 1942 Dragging of a liquid by a moving plate. *Acta Physicochimica USSR* **17**, 42–45.

Park, C.-W. & Homsy, G. M. 1984 Two-phase displacement in Hele-Shaw cells: theory. *J. Fluid Mech.* **139**, 291–308.

Quéré, D. 1999 Fluid coating on a fiber. *Annu. Rev. Fluid Mech.* **31**, 347–384.

Rabaud, M. 1994 Interface dynamics in the printer instability. *Ann. Physique* **19**, 659–690.

Rosen, J. M. 1989 *Surfactants and Interfacial Phenomenon*. Wiley.

de Ryck, A. & Quéré, D. 1993 Fibres tirées d'un bain. *C. R. Acad. Sci. (Paris) II* **316**, 891–897.

Saffman, P. G. & Taylor, G. I. 1958 The penetration of a fluid into a porous medium or Hele-Shaw cell containing a more viscous liquid. *Proc. Roy. Soc. Lond.* A **245**, 312–329.

Shen, A. Q., Gleason, B., McKinley, G. H. & Stone, H. A. 2002 Fiber coating with surfactant solutions. *Phys. Fluids* **14**, 4055–4068.

Tajima, K., Muramatsu, M. & Sakaki, T. 1970 Radiotracer studies on adsorption of surface active substance at aqueous surface. I. Accurate measurements of adsorption of tritiated sodium dodecylsulfate. *Bull. Chem. Soc. Japan* **43**, 1991–1998.

Taylor, G. I. 1934 The formation of emulsions in definable fields of flow. *Proc. R. Soc. Lond.* A **146**, 501–523.

Woolfrey, S. G., Banzon, G. M. & Groves, M. J. 1987 The effect of sodium chloride on the dynamic surface tension of sodium dodecyl sulfate. *J. Colloid Interface Sci.* **112**, 583–587.